Sensors & Transducers, Vol. 155, Issue 8, August 2013, pp. 155-161

Sensors & Transducers

http://www.sensorsportal.com

Research on Digital Robot Aided Surgery System Based on Biomechanical Information

Monan Wang, Jinke Li

Robotics Institute, Harbin University of Science and Technology, Harbin, 150080, China

Tel.: 0451-86390530

E-mail: qqwmnan@163.com

Received: 16 May 2013 /Accepted: 12 August 2013 /Published: 20 August 2013

Abstract: Aimed to develop a virtual robot aided surgery system which can represent the reality surgery process and realize force feedback by digital human tissue biomechanical information and outer force feedback instrument, human tissue geometrical and biomechanical modeling, biomechanical model calculation, force feedback instrument design, control algorithm are described. Finally, experiment was conducted after local area network is connected between haptic device control system and virtual environment. The results show this virtual robot can be controlled by master slave systems and realize visual feedback and force feedback. *Copyright © 2013 IFSA.*

Keywords: Biomechanical information, Force feedback, Robot aided surgery, Virtual surgery system, Control system.

1. Introduction

The development of modern science and technology more and more reflects the interdisciplinary characteristics. Virtual surgery, as a developing research direction, is a new field which integrates medical science, biomechanics, mechanics, materials science, computer graphics, computer vision, mathematical analysis, robotics and many other disciplines. Its purpose is to use computer technology to simulate and guide various processes involved in medical surgeries, which can be classified as preoperative, intraoperative, postoperative processes according to time, or be classified as surgical planning, surgical rehearsal, surgical teaching, surgical skills training, intraoperative guidance, postoperative rehabilitation according to surgical purpose.

In 1996, Satave [1] proposed the concept about the three generations of medical simulation system framework at the Fourth International Conference on Medical Virtual Reality. In the three generations of medical simulation system framework, the first generation medical simulation system focused on the performance of geometric characteristics of the human body, which applied the concepts of roaming and immersion to human anatomy data sets and provided a limited user interaction, has been applied to the education and training of health care workers. The physical characteristics of the different organization were taken into account in the second generation of medical simulation system during the organization modeling. The functional essence of human organs, for example, cutting off the blood vessels (physical phenomenon) may impact on blood pressure (physiological phenomenon) and then affect the normal function of other organs (physiological function), was taken into account in the third generation of medical simulation system. Overall, the third generation of medical simulation system is closest to physiological functions and biological functions of human body, and it is the ultimate research goals of medical simulation system. Currently, most the researches on virtual surgery focus on the second generation of development framework, that is physics simulation of the biomechanical properties of organ and tissue.

Orthopedic surgery is the most kinds of operation in hospitals. But precise reposition of broken bones, which is the major procedure before fixing in fracture surgery, is always challenges to most surgeons, sometimes even the experienced experts. The dragging is the popular antagonistic action on the beginning of reposition, which is used to deal with retraction and imbedding. The strength of traction should be gradually, continuously increased to avoid steep rising. The demand for pulling manner, pulling strength and distance is varied with breaking position. So it will make much sense to develop an anatomically realistic biomechanical model for surgical training, surgical rehearse and telesurgery. Especially, it is more meaningful in robot aided surgery system, as it can guide the control strategy for medical robots.

Based on the above background, this paper completed the design of digital robot-assisted surgery system based on biomechanics signal for the robot-assisted fracture traction reduction surgery platform.

2. Biomechanical Model

The force analysis of leg in tibia and fibula fracture traction reduction surgery is shown in Fig 1. Parallel robot applied traction to the human leg calcaneus by Kirschner nail and the talus was connected with the calcaneus, then was the fractured lower half fibula. Because the fractured lower half fibula is separated from the fractured upper half fibula, so the stress can't be transmitted directly but only by muscle adhered thereon. The fixing force of fractured upper half fibula was mainly derived from bracket fixed on the upper half curs as well as the strap fixed on lower half thigh. Overall, either muscle or bone was substantially exposed to a force along the direction of the lines of force, as shown by the blue line in the figure below.

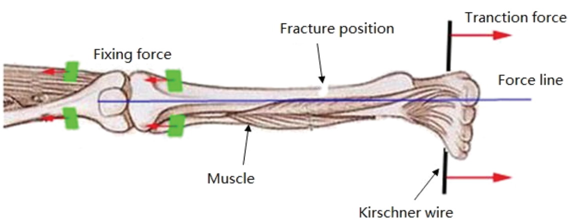

Fig. 1. The force analysis graph of leg during detracting.

Although there are many physiological tissues in human bogy leg, such as bones, muscles, nerves, blood vessels, lymph, fat, skin and so on, neither their anatomical structures nor their biomechanical properties presented in surgery differ from one another, this point is significant in the force analysis on legs through the traction reset operation, their functions are different as well. For example, the nerves, blood vessels and fact, almost have no contribution to the generation of traction during surgery, so they can be ignored in modeling process. While the bones and muscles play relatively significant roles during surgery.

2.1. Bone Biomechanical Properties Equation

The bones are generally composed of cortical bone and cancellous bone and its major components are hydroxyapatite and collagen fibers. The hydroxyapatite is very hard, its elastic modulus along the axial direction is 165 GPa; the collagen fibers do not consistent with the Hooke's law, but its tangent modulus of elasticity is about 1.24 GPa. The overall elastic modulus of the bone falls in between of the above two, the overall mechanical property is better than any of the two, because the soft collagen fibers can prevent the hard materials from brittle fracture and the hard hydroxyapatite can prevent the soft materials from yielding.

In actual surgery, X-ray was used to detect the leg bones, and we found that the bone tissue has no significant deformation. Therefore, the isotropic linear elastic model was used to define the materials to reduce the calculation amount. The following table1 is the basic material properties parameters of bone determined through research results of Jason, Zhang Ming et al, Hong Kong University of Science and Technology [2].

Table 1. Material properties and element types of bones in the finite element model.

Name	Unit type	Young's modulus	Poisson's ration
Bone	Solid185	7300	0.3

For the purposes of simplify the model and reduce the calculation amount, the isotropic linear elastic model has been widely used in simulation of biological finite element, especially in the cases of small deformation and small displacement [3]. The elastic potential energy of the isotropic material W (X) is a quadratic function of the infinitesimal strain tensor:

$$W(X)=\frac{\lambda}{2}\left(trE_L\right)^2+\mu trE_L^2, \tag{1}$$

where λ, μ are the Lame constants used to characterize the elastic constants of the elastomer, which are functions of the elastic modulus E and Poisson's ratio.

2.2. Muscle Biomechanical Properties Equation

The muscle contains many muscle fibers which are small subunits, and this is the reason the muscle surface has striped appearance. The muscle fiber is about a few centimeters of cylindrical structure, it has many long strips of subunits inside, namely, myofibril. According to the currently accepted mechanism of muscle contraction – myofilament sliding theory, these myofibrils are the real elements of contraction mechanism. When the muscle is in a resting state (without muscle activities dominated by nerve awareness), the elasticity of muscle is mainly generated by muscle myofibrils of the muscle. The muscle myofibrils mechanically arranged in parallel to form the parallel elastomeric element. Therefore, during the construction of the finite element model of the muscle fibers, the anatomical structure of the finite element units should be consistent with that of the muscle fibers on both shape and size as much as possible.

The linear elastic materials model was used for the representative tendon of beam element to show the biomechanical properties. The Mooney-Rivlin incompressible hyperelastic model was used for the muscle fiber model, which could be well described the mechanical properties with deformation less than 150 % and can fully meet the property computing needs of the practical application. The Mooney-Rivlin two-parameter model was used in this model in order to guarantee the computational efficiency. The formula is as follows:

$$W = C_{10}(\overline{I_1} - 3) + C_{01}(\overline{I_2} - 3) + \frac{1}{d}(J-1)^2 , \quad (2)$$

where W is the strain energy density function. C_{10}, C_{01} are the mechanical properties constants. $\overline{I_1}$ and $\overline{I_2}$ are the first and second deformation tensor invariants respectively.

According to the research results of the computer science professor J. Teran of Stanford University [4], the material parameters of the muscle fiber and the tendon in the muscle model were determined in Table 2.

Table 2. Material properties and element types of muscles in the finite element model.

Component	Element type	Young's modulus E (MPa)	Cross-sectional area (mm^2)
Muscle	Solid185	Mooney-Rivlin Hyper elastic model	
Tendon	Link10	350	290.7

2.3. The Biomechanical Properties Equation of the other Soft Tissues

The other soft tissues including fat, blood vessels, nerve and so on. Due to their CT images are more blurred than that of the muscles, we can't get the three-dimensional reconstruction. They were all regarded as an isotropic material in this model, besides the bones, muscles and tendons, all other space surrounded by skin are filled with such soft tissue.

Generally, the stress-strain relations of these soft tissues do not meet the Hooke's law and can obtained through experiment only. As shown in Fig. 2, the experiment data were obtained by the Lemmon et al, Health Research Center of Pennsylvania State University [5]. Wherein, the F2, F3 and F5 respectively refer to the stress-curves at 2-fold, 3- fold and 5-fold normal tissue stiffness.

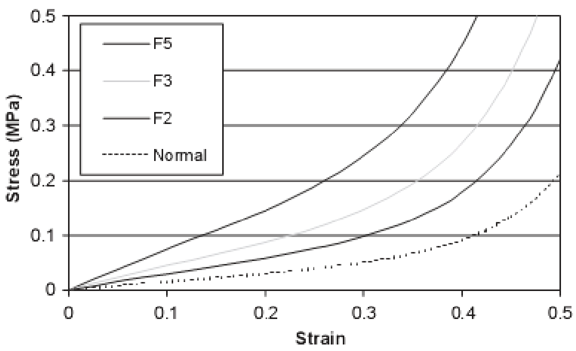

Fig. 2. Nonlinear stress–strain response of soft tissue.

The second-order Polynomial Form hyperelastic model was used to simulate the material properties of the soft tissue.

$$W = \sum_{i+j=1}^{N} C_{ij}(\overline{I_1} - 3)^i(\overline{I_2} - 3)^j + \sum_{k=1}^{N} \frac{1}{d_k}(J-1)^{2k} \quad (3)$$

Where W is the strain energy density function. C_{ij} is the mechanical properties constant. $\overline{I_1}$ and $\overline{I_2}$ are the first and second deformation tensor invariants respectively. Available parameters are shown in Table 3.

Table 3. The coefficients of the hyperelastic material model used for the encapsulated soft tissue.

Coeffi-cients	normal	F2	F3	F5
C_{10}	0.08556	0.17113	0.25669	0.42782
C_{01}	-0.05841	-0.11683	-0.17524	-0.29207
C_{20}	0.03900	0.07800	0.11700	0.19499
C_{11}	-0.02319	-0.04638	-0.06957	-0.11594
C_{02}	0.00851	0.01702	0.02553	0.04256
D_1	3.65273	1.82636	1.21758	0.73055
D_2	0.00000	0.00000	0.00000	0.00000

3. Finite Element Model

The main task in reset operation of bone is to separate the two broken leg bones and then align them. As shown in Fig. 3, the upper half bone of the lower leg was fixed to the bracket with a bandage. The lower half bone was fixed on the parallel robot using the Kirschner nail.

Fig. 3. Load conditions in surgery.

Fig. 4 shows the finite element model determined by actual state in surgery. On the fixed point with bandages on upper half of the lower leg, the degree of freedom was defined as 0. Two forces were applied to both ends of the Kirschner nail with the same direction and half-intensity of traction force of parallel robot. Fig. 5 shows obtaining the information between position and the force according to the finite element biomechanics calculation.

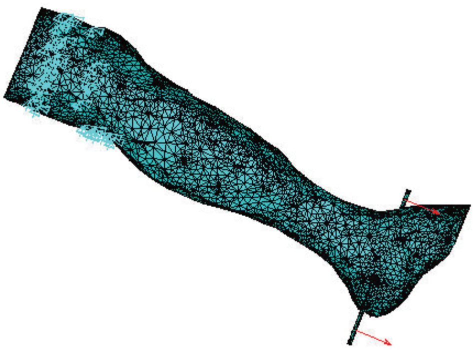

Fig. 4. Finite element model.

4. Design of Force Feedback System

4.1. Design of Haptic Device Mechanism

The haptic device was shown in Fig. 6. This parallel haptic device was consisted of moving platform and the base connected by the kinematic chains composed of three groups of the compression apparatus and connecting rod, the stiffness of this parallel mechanism was good, and its structure was compact, ensuring its sufficient degrees of freedom.

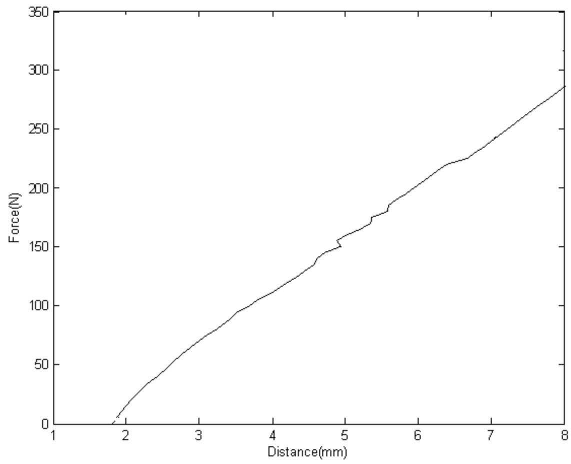

Fig. 5. Force-distance curve.

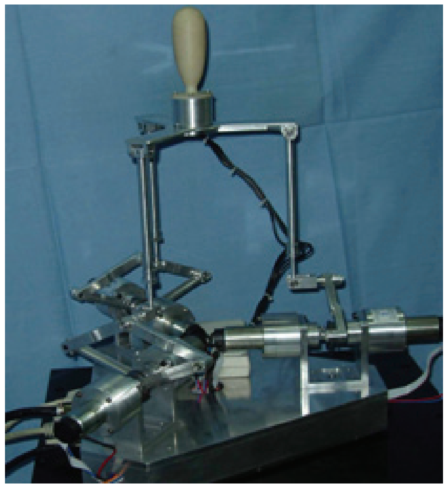

Fig. 6. Parallel haptic device.

Due to the motor fixed on base, the inertia of this mechanism was greatly reduced, and the force feedback property was enhanced. Through the application of pantograph structure, and the connection between RRR type kinematic pair and connecting rod as well as the connection between the other end of the connecting rod and upper mounting plate by a revolute pair, thus the parallelogram compression apparatus link mechanism was limited to rotate within three planes parallel to base, thus the manipulation on the rotation angle of connecting rod of base motor, the position and shape can be adjusted. Six-axis driving motor used DC torque motor, through the connection between harmonic reducer and various link mechanism, and the drive of motor by DC and the actuation of harmonic reducer, the systematic backlash can be avoided, and the motion accuracy of haptic device can be improved.

Further, the structure of this mechanism is simple, and its manufacturing and operation is relatively easy. Its accuracy can also be guaranteed. The parameters of the workspace of the haptic device are shown in Table 4.

Table 4. Workspace parameters of the haptic device.

Rotation angle vertical to X-axis	Rotation angle vertical to Y-axis	Rotation angle vertical to Z-axis	X-axis	Y-axis	Z-axis
≤35⁰	≤35⁰	≤35⁰	±150 mm	±150 mm	180-350 mm

4.2. Haptic Device Control Structure

In order to achieve master-slave mode of force feedback and meet the requirements such as haptic device position accuracy, and rapidity, based on the ideology of the position loop force control, the control system used computer cascaded structure, which was divided into four levels: current loop, velocity closed loop, position closed loop and force closed loop. Force closed loop contains position loop, the realization of force control is based on the realization of position control, as can be seen from Fig. 7, the structural relationships between four closed loops were shown.

4.3. Design and Implementation of Systemic Control Arithmetic

The control structure based on position loop was applied to the parallel haptic device control system. The feedback force produced by driven robot and the human tissue effect was taken as the desired force of the system F_d, the interaction force of the operator and the haptic device detected by the force sensor on the parallel haptic device was F. The difference between the F_d and F was taken as the system control inputs, so as to form a closed loop servo of system force. The structure is shown in Fig. 8. The characteristics of its control structure include [6-10]:

1) The control inputs transform the force control into the robot's speed control similar to the form of damping control, rather than explicitly act on each joint in form of torque.

2) The force feedback directly compares with the desired force and takes the difference as the input of the force controller, rather than become the input item of the speed command, thereby forming a force control servo loop.

3) The movement control of main hand in workspace under the dynamics decoupling conditions, the multidimensional force of workspace can be decomposed into force control of dimensional independent force, and a variety of control law of force control can be achieved.

5. Achievement of Digitization Robot-Assisted Surgery System Based on Biomechanics Signal

The virtual surgery system is an integration of virtual reality technology and the modern medicine.

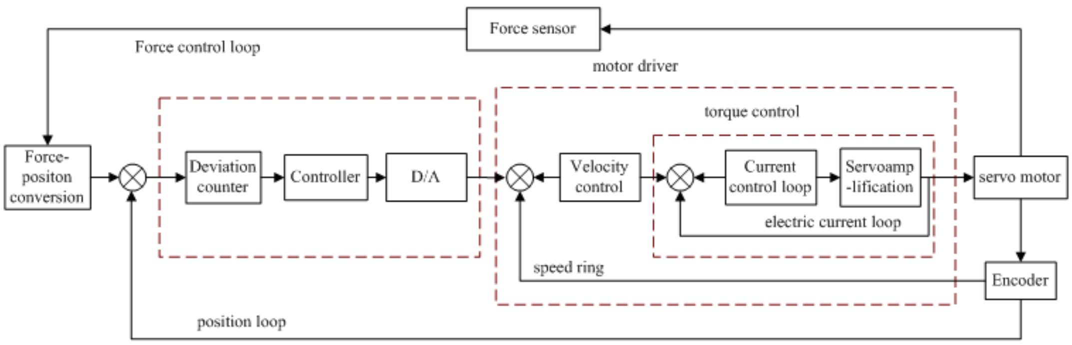

Fig. 7. Layers of control system.

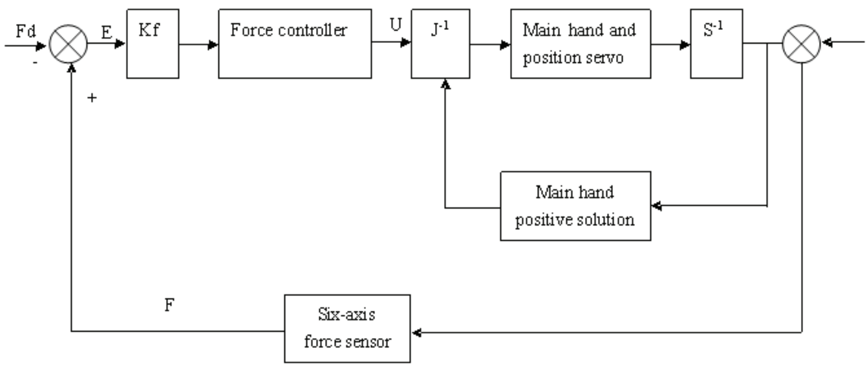

Fig. 8. Constructor of control arithmetic.

The users can feel immersion (such as sense of vision, force and tactile), realism and real-time interaction in a virtual environment, and the object's status in virtual environment can be changed through virtual tools [11-16]. The framework of virtual surgery system is showed in Fig. 9 and master slave control operation system is showed in Fig. 10. In the experiment, when the haptic device control system and virtual environment were successfully connected through the LAN, the haptic device control system will collect the movement positions and postures of the parallel haptic device every 15 ms and send the data to the virtual environment end through network, at the same time, the virtual environment end will create a separate thread to receive signals, the 6 positions and postures data was loaded into the paralleled surgery robot platform after the signals were successfully analyzed in accordance with the established way, thus paralleled surgery robot platform produced movement consistent with the haptic device. The displacement between the broken bones can be calculated based on the movement of the parallel surgery robot platform, and the force required in the current circumstance can be obtained after input the displacement into the neural network model based on the learning of finite element model, and the force required can be fed back to the operator through the parallel haptic device, thus completed a full closed loop.

The operator will also get visual feedback from the virtual environment when got the force feedback. The parallel robot in virtual environment will update the position and posture based on the signal sent by outer parallel haptic device. In addition, the force feedback can be displayed on the operator interface in real-time, it can be also reflected intuitively through the JFreeChart control and bone color changes, as shown in Fig. 11.

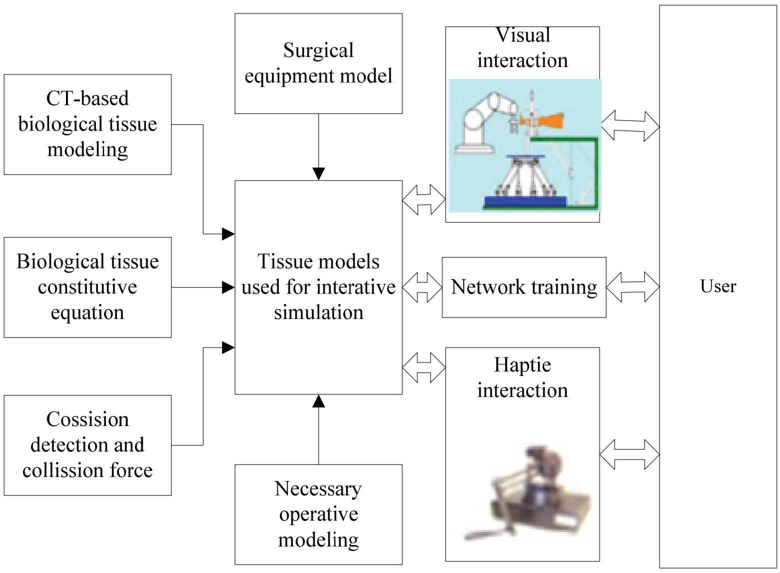

Fig. 9. Virtual surgery system.

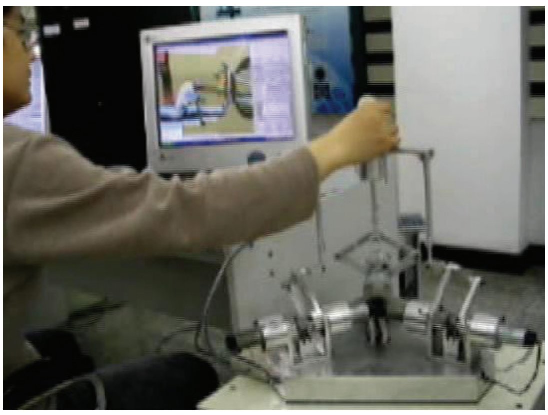

Fig. 10. Master slave control operation.

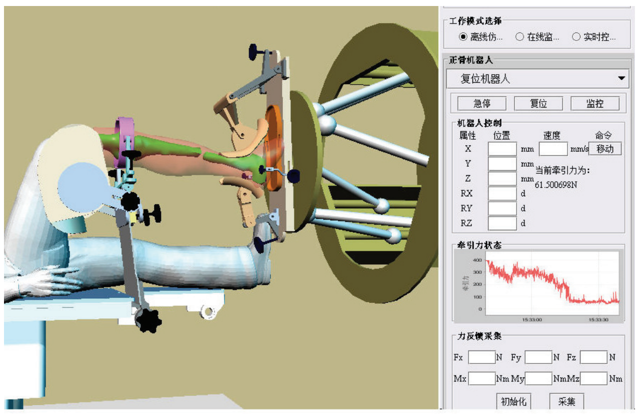

Fig. 11. Interface of virtual surgery system.

6. Conclusions

Through the establishment of biomechanics characteristic equation, finite element calculation of biomechanical equations and the design of force feedback device, digitization robot-assisted surgery system based on the biomechanical signal was achieved, the system is able to obtain force position changes information and visual feedback in surgery, and the robot control parameters can be adjusted at any moment based on the feedback information. The program also can be applied to non-robot surgery system, the users can feel the force status of surgical equipment during surgical procedures through the feedback device. The major conclusions include:

1) Multi-level human tissue biomechanical models of bone, tendon, muscle, skin and other soft tissues were established through the analysis of force status of corresponding human tissues in the bonesetting experiments.

2) The mechanical body design, control system design of the haptic feedback device were complete and design of systemic control arithmetic were achieved, the virtual master-slave operation tests on digitization robot-assisted surgery system based on biomechanics signal were established, and the feasibility of parallel haptic device control arithmetic was verified through completing the relevant tasks using parallel haptic device control the virtual robot.

Acknowledgements

The authors would like to thank for the financial support of NSFC(61073144\61272387) and Chang Jiang Scholar Candidates Programme for Provincial Universities in Heilongjiang (2013CJHB007).

References

[1]. R. Satava, Medical Virtual Reality: The Current status of the future. *in Proceedings if the 4th Conference on Medicine Meets Virtual Reality (MMVR IV)*, San Diego, CA, 19-22 January 1996, pp. 100-106.

[2]. T. C. Jason, M. Zhang, A. K. Leung, Y. B. Fan, Three-dimensional finite element analysis of the foot during standing-a material sensitivity study, *Journal of Biomechanics,* Vol. 38, 2005, pp. 1045-1054.

[3]. A. D. Speirs, M. O. Heller, G. N. Duda, W. R. Taylor, Physiologically based boundary conditions in finite element modeling, *Journal of Biomechanics*, Issue 10, 2007, pp. 2318-2323.

[4]. J. Teran, E. Sifakis, S. S. Blemker, V. Ng-Thow-Hing, C. Lau, R. Fedkiw, Creating and simulating skeletal muscle from the visible human data set, *IEEE Transactions Visual Computer Graphics,* Vol. 13, Issue 11, 2005, pp. 317-328.

[5]. D. Lemmon, T. Y. Shiang, A. Hashmi, J. S. Ulbrecht, P. R. Cavanagh, The effect of insoles in therapeutic footwear: a finite-element approach, *Journal of Biomechanics*, Vol. 30, 1997, pp. 615-620.

[6]. J. J. Xi, W. X. Tan, S. H. Li, Research on disease pattern resemblance recognition model, *Computer Engineering*, Vol. 36, Issue 8, 2010, pp. 56-60.

[7]. C. Y. Fan, C. C. Hsu, C. K. Chao, Biomechanical comparisons of different posterior instrumentation constructs after two-level ALIF: a finite element study, *Medical Engineering & Physics*, Vol. 32, Issue 2, 2010, pp. 203-211.

[8]. A. Rohlmann, T. Zander, G. Bergmann, Effects of fusion-bone stiffness on the mechanical behavior of the lumbar spine after vertebral body replacement, *Clin Biomech*, Vol. 21, Issue 3, 2006, pp. 221-227.

[9]. J. C. Le Huec, V. Lafage, X. Bonnet, Validated finite element analysis of the maverick total disc prosthesis, *Journal of Spinal Disorders & Techniques*, Vol. 23, Issue 4, 2010, pp. 249-257.

[10]. J. M. García-Aznar, J. H. Kuiper, M. J. Gómez-Benito, M. Doblaré, J. B. Richardson, D. R. Epari, H. Schell, H. J. Bail, G. N. Duda, Instability prolongs the chondral phase during bone healing in sheep, *Bone*, Vol. 38, 2006, pp. 864-870.

[11]. L. Qin, Mechanical stimulation enhances osteogenesis and bone generation, *Journal of Medical Biomechanics*, Vol. 27, Issue 2, 2012, pp. 129-131.

[12]. D. H. Sun, Y. Wang, Robot control technology. *China Machine Press*, 1997.

[13]. M. N. Wang, H. S. Guo, Fixation for femoral neck fracture based on nonlinear materials, *Journal of Medical Biomechanics*, Vol. 27, Issue 2, 2012, pp. 152-158.

[14]. Y. H. Yin, Z. X. Wei, X. X. Huang, Force sensing and force control technology for intelligent machine system. *Journal of Medical Biomechanics*, Vol. 20, Issue 2, 2011, pp. 90-92.

[15]. R. L. Williams, M. A. Mark, Naturally transitioning rate-to-force control, *ASME Design Engineering Technical Conference*, Atlanta, U.S., 9-12 September 1998, pp. 1-6.

[16]. Y. Cheng, The design and accomplishment of position servo systems based on computer control, Master Thesis, *Nanjing University of Aeronautics and Astronautics*, 2003.